Radar ATR of Maritime Targets

Hartmut Schimpf
FhG Fraunhofer-Institut für Hochfrequenzphysik und Radartechnik (FHR)
Neuenahrer Straße 20, D-53343 Wachtberg – Werthhoven, GERMANY

hartmut.schimpf@fhr.fraunhofer.de

ABSTRACT

A short overview of ship ATR schemes in general is followed by an in-depth analysis of the use of HRR profiles under shallow depression angles that suffer from the influence of multipath and atmospheric duct phenomena. The critical issue of defining appropriate training and testing profiles or feature vectors derived therefrom is addressed. Some ideas how to mitigate the influence of multipath in order to arrive at stable feature estimates are presented.

1. INTRODUCTION

For commercial ship traffic the Automatic Identification System (AIS) is obligatory for all vessels above a certain size and thus warrants their cooperative classification and even identification. However, for smaller craft and especially for non-cooperative objects with hostile intent, the classification has to rely on classical approaches of automatic target recognition (ATR) which mostly are based on radar due to its day/night and all-weather capabilities. This leads to applications like coastal surveillance for border control, the protection of harbour installations, ship self defence or the suppression of drug trafficking, where the classification of ships by means of ATR schemes becomes more and more important. This is especially true in times of asymmetric (terrorist) threat and piracy.

With a modern high resolution radar one has the choice of two different ways of target imaging. The first is 2-D imaging, either from an airborne (SAR) or from a ground-based platform (ISAR). The latter depends on the relative motion of the target itself and therefore may be difficult in the case of non-cooperative targets. The desired axis of rotation should be vertical which may not be the case when high sea states cause strong roll and pitch motion for smaller ships. Moreover, when the hostile ship is approaching or receding on a straight course, there is no relative rotation that lends itself to ISAR exploitation.

Typical 2-D approaches start with the imaging process [6], followed by a detection and segmentation stage [7]. From the target image proper, features are extracted for the subsequent target classification. Valuable information is obtained from polarimetry in connection with SAR imaging (PolSAR) [7][8][12] which is used for target / background separation in the detection stage, and for the characterisation of special scattering mechanisms that support classification. If available, even interferometry [9] can be added (PolInSAR). Bon et al. [10] reconstruct the 3-D structure of dominant scatterers by means of Pauli decomposition and classify the ship via pattern matching against a reference data base. Ship ATR based on ISAR imaging and features that are derived therefrom is described by Pastina [15][16] and Musman [17].

While 2-D imaging is the most promising approach in the case of airborne and spaceborne radar sensors with SAR capabilities, the second possible approach is 1-D imaging obtained by means of high range resolution (HRR) profiles. This circumvents all the difficulties of determining an axis of rotation for ISAR imaging or the need of a moving sensor platform for SAR imaging. Therefore, its use is more realistic for ground based radar. Also, it seems that HRR profiles are more robust against aspect angle variations than ISAR images as was found by Menon et al.[11]. The authors start their approach with ISAR images but then sum all intensities within each range bin to end up with HRR profiles for further use.

The range resolution that determines the HRR profiles depends on the radar bandwidth. The shape of the HRR profile is a function of aspect angle, but also on range due to an increasing clutter contribution in a real-beam situation, and due to the influence of multipath at shallow depression angles. This will have severe consequences for the computation of features that are used for the classification of a ship. Important features that can be used for classification are those which use the geometry of ships like length and width. Also, the ATR algorithm can use features that describe the structure of dominant scattering centers on the ship, their relative locations and amplitudes as they appear in the HRR profile [13].

Close inspection of all possible scenarios leads to the conclusion that the problem of maritime ATR falls in two main classes. On one side there are airborne or spaceborne sensor platforms that are moving and therefore are able to perform 2-D imaging. They observe under steep depression angles and thus do not suffer from multipath. Consequently, they can generate high fidelity images that can be used for pattern matching with objects from a library, or for classical similarity tests in some feature space. Hence, essentially all the methods developed for land targets can be applied with the difference that the surrounding clutter is non-stationary and highly variable depending on wind conditions and the sea state. – On the other side, there are stationary ground based (including ship based) radars that depend on real-beam cross-range resolution and therefore will evaluate HRR profiles. Due to the shallow depression angles and the presence of the marine boundary layer there will be multipath and atmospheric duct phenomena that cause strongly range dependent signatures. The challenge consists in defining appropriate training and testing vectors because a reference to existing libraries is extremely difficult using local estimates. This latter topic, because it is unique to the maritime domain, will be the subject of the following lecture.

2. THE USE OF HIGH RANGE RESOLUTION (HRR) PROFILES FOR ATR

HRR profiles are naturally applicable to the situation of a hostile ship that is approaching directly. In that case, there is no change of aspect angle that would support the creation of an ISAR image. Rather, the full HRR profile of the ship is seen without any projection effects. However, several problems make the exploitation of HRR profiles rather difficult:

- shadowing (self-masking) effects due to a very low depression angle δ. This is especially the case in a maritime scenario where δ usually is close to 0°. The highest parts on a ship's body are mostly close to its center so that either the bow or the stern region may be occluded. Consequently, this problem is based on the shape of the target and on the aspect angle and cannot be influenced by an appropriate choice of radar parameters.

- low signal-to-noise ratio due to a very large slant range

- low signal-to-clutter ratio due to the large angular extent of the footprint in a real-beam situation: while the scatterers on the ship keep their RCS, the RCS of the clutter cell increases proportional to the distance R.

- multiple target situations due to the large angular extent of the footprint in a real-beam situation: the further away a ship is the more likely it becomes that a second ship at a similar range may enter the beam as well. A 2° beam has a cross-range extent of 350m at 10km range! This can only be overcome by constant monitoring of the surveyed area.

- The occurrence of spray near the bow and wakes near the stern of the ship which will contribute to its signature

As will be seen in ch.3 the computation of ATR features from HRR profiles is based on a "minimum bounding range interval" (MBRI) that is defined by the range extent of a certain number N_{st} of dominant scatterers. The question is how to determine these. As one sees from fig.1, in the case of high range resolution (the profile shown was taken at 17GHz with 300MHz bandwidth corresponding to 0.5m range resolution) most dominant scatterers create peaks of a certain width which may well be more than one range cell. Thus it might happen that "the 2nd strongest RCS" corresponds to the flank of the peak with the strongest RCS and physically would not represent a scatterer of its own. Therefore, the original HRR profiles have to be transformed into "ensembles of peaks" based on the following conditions:

- A "peak" must have at least 2 values of lower RCS on both sides
- The peak RCS must exceed a threshold that is given by the average sea clutter level

Fig.2 shows which of the HRR lines are recognized as individual peaks (marked by red asterisks). This leads to an equivalent "peak profile" (fig.3) on which the ATR features are calculated.

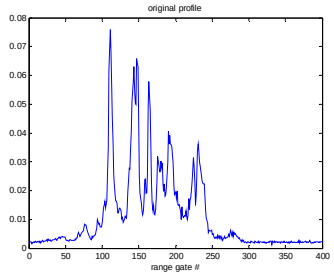

Figure 1: typical HRR profile measured at 17GHz (RCS/m^2), 0.5m resolution

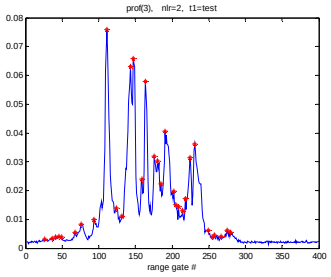

Figure 2: same profile as in fig.3 with peaks marked by red asterisks

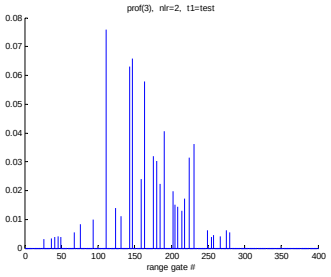

Figure 3: profile from fig.3 transformed into peak profile as used for feature computation

3. THE DERIVATION OF ATR FEATURES FROM HRR PROFILES

3.1. Length Estimate

Out of all recognition features based on scatterer geometry that one might think of, "length" seems to be the simplest and most straightforward. However, the estimation of the length of an extended radar target – be it a land vehicle, an aircraft, or a ship – is a non-trivial task [4].

Several problems like shadowing, and a low signal-to-noise and signal-to-clutter ratio make the exploitation of HRR profiles rather difficult as described in ch.2. Information about the target can only come from scatterers that contribute to the backscatter signal. The latter is not the case for those parts of the target that are masked by others, and it is not the case for scatterers that although physically belonging to the target and illuminated by the radar cause specular scattering away from the radar antenna and hence are invisible. Even estimating the length of a ship will be subject to error when characteristic scatterers near the bow or the stern fall below a certain detection threshold due to multi-path (figs.4 and 11).

Based on HRR profiles, "length" can be defined in several ways [4]. Each one has its advantages and disadvantages, and the results normally are not identical. In the case of ships, two different methods were

applied [3]. The first one (L_a) equals the extent of the smallest window containing x<100% of the total energy of the profile and uses an adaptive threshold that is based on the mean and standard deviation of the sea clutter RCS. This takes into account that the sea clutter RCS increases proportional to R due to the real beam situation. The mean m_{clut} and standard deviation s_{clut} are determined from the n_{clut} lowest values of the sorted HRR profile, N_{Thr} is a "CFAR-factor", then the threshold is defined as

$$Thr = m_{clut} + N_{Thr} * s_{clut}$$

Good results were obtained with n_{clut}=140 and N_{Thr}=10 in profiles of length N_{HRR}=200, and with Δr=1.5 meters, i.e. a maximum range extent of 90m of a ship could be accommodated. The "Planet" had a length of 73 meters corresponding to 49 range cells.

The second method (L_b) is quite different. One starts with a window containing a small number of the N_{st} strongest peaks of the HRR profile (usually N_{st} =3 or 4). Step by step one increases the window size by one cell by incorporating the next adjacent cell (before or behind the present window) on the side with the higher RCS estimate. This estimate is based on a power sum of three range cells in order to avoid extreme local minima. At each step the relative power increase $\Delta_i = p_i/\Sigma p_i$ is determined. The window size has reached the final "length" L_b as soon as Δ_i stays permanently below a certain threshold. A value of 0.01 was found to be useful.

3.2. Position specific matrices (PSMs)

The concept of PSMs was developed for the description of gene sequences in DNA analysis (cf. Cotuk et al. [13]). This technique does not derive single features from the HRR profile but rather treats HRR profiles as an entity. In the same way as a DNA molecule can be represented by a sequence of letters, where each position in the sequence is equal to one of four possible letters, an HRR profile can be represented by a sequence of RCS amplitude values. Working with PSMs comprises the following important steps:

- Determination of the length N_p of the ship profile
- Alignment of HRR profiles
- Quantisation into N_q levels
- Creation of reference PSMs (one per class) from a series of N_t profiles
- Comparison of the quantised test profile to the reference PSMs
- Determination of a figure of merit (FoM) to quantify the degree of similarity
- Classification: the test profile is assigned the class that obtained the highest FoM.

Determination of length: in a long HRR profile, most of the range cells contain only clutter. The cells that belong to the target ship have to be identified, because only these are important for the subsequent processing.

Alignment: HRR profiles in a time sequence can only be compared to each other range cell by range cell which requires careful alignment. Also, creation of the PSM depends crucially on correct alignment.

Quantisation: in the case of HRR profiles, there are not only four possible values as in the DNA case, but rather a number of N_q levels that are created artificially by quantising the more or less continuous range of RCS values. Cotuk chose a value of N_q=30 without giving a rationale or claiming this to be an optimized value. Applying this method to ships [19], it was found that the choice of N_q depends on whether the RCS data are used in linear or in dB space. In the first case, due to the high dynamic range, N_q has to be quite large (several hundred or even 1000) in order to accommodate single dominant scatterers. Therefore, it is advantageous to work in dB space. In that case, a value of N_q=10 is sufficient as can be seen by comparing fig.4 (b) (full dynamic range) and (c) (quantisation to 10 levels). All the structure of the HRR profiles necessary for classification has been preserved. A small value of N_q has the advantage of needing only limited computing power by handling PSMs of moderate size .

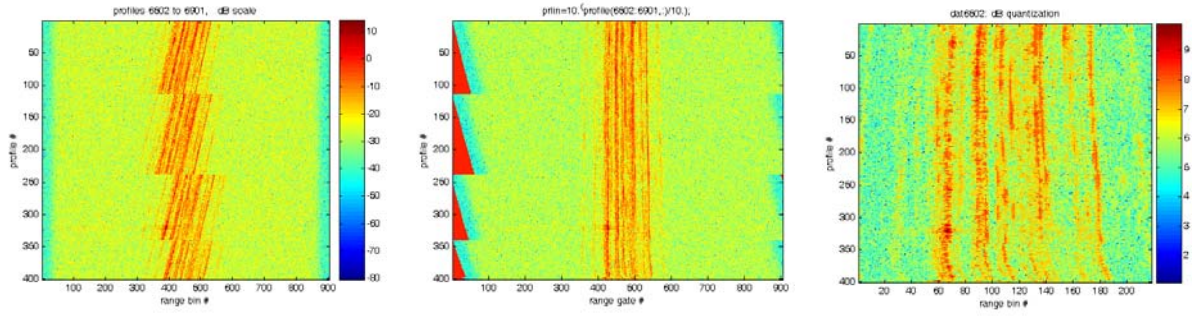

Figure 4: Series of 400 HRR profiles before (left) and after (center) alignment, both with same scale dBm2. The right image shows 208 range cells belonging to the ship, quantised into 10 levels.

Creation of reference PSMs: After having determined the length N_p of the HRR profiles, and after having performed the alignment a PSM with N_q rows and N_p columns is created. For this purpose one takes a training set of N_t profiles and inserts the frequency of occurrence of each quantised RCS level into the PSM. Stated otherwise, when RCS level "m" (out of N_q possible values) occurs in range cell "n" (out of N_p possible values) then the counter in element PSM(m,n) is increased by one. This provides us with a reference PSM in which the sum of all entries within each column is equal to N_t. This means that the highest value of any entry is less or equal to N_t. This maximum value N_t is reached only when all RCS values of the respective range cell have the same quantisation value.

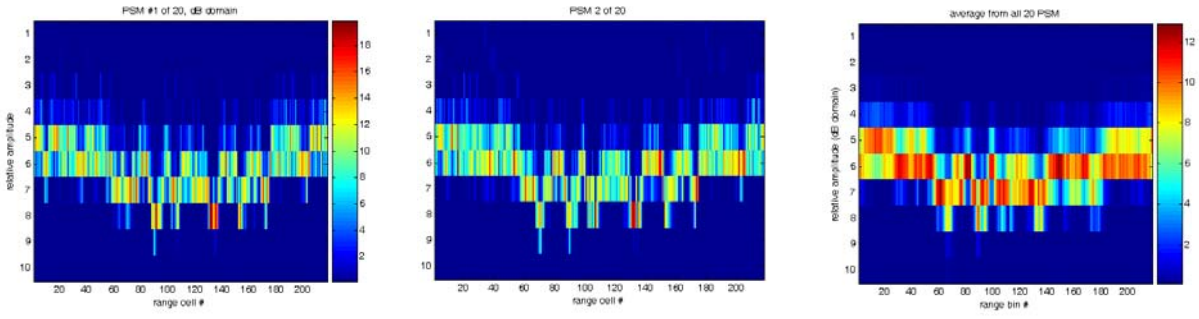

Figure 5: PSMs #1 (left) and #2 (center), scale from 0 to 20. The averaged PSM (right) has a scale from 0 to 13, hence has considerably lower values.

The example shown in fig.5 was constructed on the basis of a series of 400 consecutive HRR profiles of length N_p=208. They were subdivided in groups of 20 profiles each so that 20 different PSMs could be created with the following parameters: N_q=10, N_t=20, N_p=208. On the left and in the center of fig.5 we see the first and second PSM, respectively. On the right is shown an average of all 20 PSMs. There is a high

degree of similarity, but no identity. Also, the fact that only few range cells out of 208 reach a count close to N_t=20 (the possible maximum) gives a hint that the HRR profiles show considerable variability.

Compare the quantised test profile to the reference PSMs: How can these PSMs be used for classification? For each target class we need one reference PSM. The target under test is represented by its HRR profile (out of a series of profiles) which is quantised in the same way as the training profiles. This quantised HRR test profile (fig.6, left) corresponds to a test PSM that contains only one's in the respective positions (fig.6, right) and that has now to be compared to the reference PSM of each target class. This comparison is done cell by cell for every matrix element. A high score in PSM_{ref} at a position given by PSM_{test} means high similarity, a low or zero score means dissimilarity.

Determine a figure of merit: In order to quantify the degree of similarity, some "likelihood measure" or "figure of merit" (FoM) has to be defined. Cotuk et al. use a "likelihood score" (LS) by identifying a single row for each column of the reference PSM for the hypothesized class. This row corresponds to the quantized amplitude level in the observed profile at that spatial location as indicated by the test PSM. They then take the product of all these matrix entries because they argue that the entries in a PSM are proportional to the estimated probability of observing a particular RCS level at that position. However, a product is zero as soon as any single one of its factors is zero. Therefore, the likelihood score is zero as soon as the test PSM hits an empty entry anywhere in the reference PSM although all the remaining positions may be in perfect agreement. For this reason the LS as defined by Cotuk is not well suited for comparing different degrees of similarity, especially for rather long HRR profiles (in our example N_p=208).

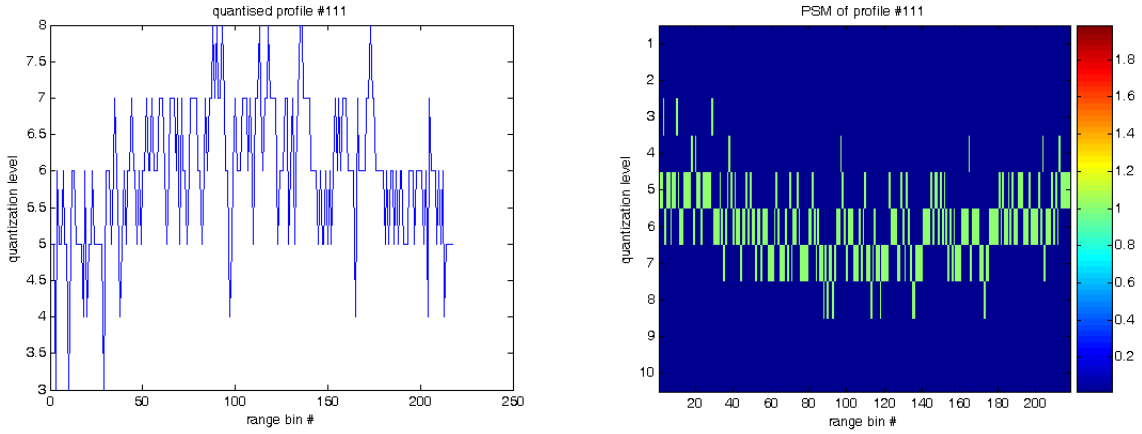

Figure 6: Quantised HRR profile (left) and its representation by a PSM (right).

We therefore propose a figure of merit (FoM) to quantify the degree of similarity that is given by

$$FoM = \sum_{i=1}^{N_q} \sum_{j=1}^{N_p} PSM_{test}(i,j) \cdot PSM_{ref}(i,j)$$

which means the element-wise product of the test PSM (PSM_{test}) and the reference PSM (PSM_{ref}). The highest possible value for FoM is $N_t \cdot N_p$, therefore, a normalised FoM may be defined as $FoM/(N_t \cdot N_p)$.

Classification: If reference PSMs are available for several different classes, then the profile under test is assigned to the class with the highest FoM.

3.3. Other examples of ATR features

Based on geometrical relations and amplitude ratios of dominant scatterers in the MBRI one can define ATR features of different types, mainly geometrical, statistical, or structural. The following set of features [21] that will be analysed in more detail in ch.5.3 are not meant to be "best" features, but rather "generic" features that may be typical for any HRR profile based ATR scheme. They are all based on HRR profiles of the ships, measured with a single polarization (H on transmit and receive). The main criteria for feature construction are

- Features must not depend on absolute RCS, i.e. no radiometric calibration is required
- Features should cover different properties of the HRR profile, e.g. geometry, statistics, and structure of the ensemble of dominant scatterers

The features that are used in the present paper are Ft1 to Ft14 as described below. Some of them were already assessed in former analysis [3][18]

- Ft1 = range extent of N_{st} strongest scatterers in the HRR profile. This range extent at the same time defines the "minimum bounding range interval" (MBRI) on which all other features are computed
- Ft2 = mean/std.dev. of RCS values within MBRI
- Ft3 = power sum of N_{pwr} strongest scatterers / power sum of all scatterers within MBRI, it describes the contribution of a few dominant scatterers to the MBRI
- Ft4 = log10(strongest RCS/N_{pos}-strongest RCS) describing the "decay" of RCS values
- Ft5 = log10(highest RCS / lowest RCS) out of N_{st} strongest scatterers
- Ft6 = relative distance between the two strongest scatterers w.r.t. range extent of MBRI
- Ft7 = slope of straight line fit of RCS (in dB) of n-th strongest scatterer (normalized to highest RCS) vs. range extent of n strongest scatterers (n=2…N_{st})
- Ft8 = shift of same fit as in Ft7
- Ft9, Ft10 = slope & shift of straight line fit to normalized RCS of N_{st} strongest scatterers (in dB) in descending order
- Ft11 to Ft14 = coefficients of cubical fit to normalized power sum of n strongest scatterers (n=1…N_{st})

For the present analysis (ch.5.3) the following parameters were chosen: N_{st}=10, N_{pwr}=5, and N_{pos}=5. Ft1 and Ft6 are of type geometrical, Ft2 statistical, all others of type structural, describing the relative RCS values and RCS ratios of dominant scatterers.

3.4. Choosing sets of uncorrelated features

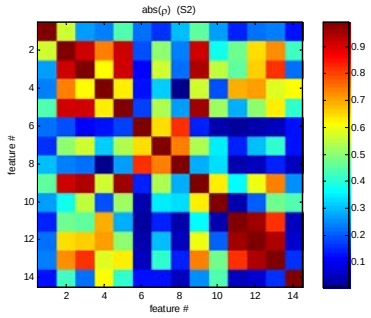

Figure 7: cross correlation coefficients abs(ρ)∈[0 1] between all 14 features

Of course, not all of the above defined features are independent of each other. In order to find out which ones may be combined to sets of features the easiest way is to look at their cross correlation coefficients ρ. A typical example for abs(ρ)∈[0 1] is shown in fig.7 based on a simulated ship with fixed orientation, but at many different range positions. From this one can conclude that good sets of uncorrelated features are 1, 4, 8, 14 or 2, 6, 14 or 7, 11, 14 among many other possibilities.

4. SHIP ATR UNDER THE INFLUENCE OF MULTIPATH

4.1. What is multipath?

The task of detecting and classifying a ship very often has to be performed by sensors that are located close to the sea surface. This can either be onboard a ship or in a stationary location on the coast. Due to the shallow looking angles and to the special conditions of the sea surface and of the atmosphere immediately above the sea surface (marine boundary layer), the influence of multi-path and of atmospheric duct phenomena plays an important role when measuring a ship's radar signature. This is because scatterers are affected in a different way depending on their height above the sea surface. As a consequence, the amplitude relations between different scatterers at different heights on a ship depend strongly on the distance between the radar and the ship that has to be classified. This means that high range resolution (HRR) profiles and ISAR images that are the basis of extracting ATR features, are not only a function of target aspect but also a function of the distance to the target under distinct atmospheric conditions and sea states [2]. - In the ideal case of mirror-like reflection and without taking into account atmospheric effects, multipath is described by means of the path difference Δ between direct and reflected ray

$$\Delta = \frac{2Hh}{s} \cdot \frac{1 + \frac{H^2 + h^2}{2R} \cdot \frac{s^2}{2Hh(H+h)}}{1 - \frac{2Hh}{s^2}} \qquad (1)$$

(H = antenna height, h = scatterer height, R = Earth's radius, s = slant range between antenna and scatterer). The interference between the direct and the reflected ray leads to the complex voltage

$$V = A \cdot e^{i(kx - \omega t)} \left(1 + f \cdot e^{i\frac{4\pi}{\lambda}\Delta}\right) \qquad (2)$$

where f∈[0 1] takes into account the surface roughness via a reduced reflectivity. This is shown in fig.8 for H=19m and a radar frequency of 35Ghz (λ=8.6 mm). If atmospheric effects and duct phenomena in the

marine boundary layer are included a closed analytical solution is no longer available. Rather, one has to depend on modelling software like TERPEM [5] which yields results as shown in fig.9. The overall appearance, of course, is similar to the “undisturbed” case, but the behaviour in detail may be completely different.

Reality, as it demonstrates itself in measured HRR ship profiles is even more complicated. If we imagine the sea surface as a multitude of non-stationary reflecting facets with different inclinations then even the concept of one reflected ray interfering with the direct ray fails. Wave facets closer to the ship but inclined towards the radar as well as facets closer to the radar but inclined towards the ship may as well act as the origin of additional reflected paths. Also, facets with varying inclination may cause scatterers to show up that were not visible before: parts of the ship that have the same angle w.r.t. vertical as the wave facet has w.r.t. horizontal may lead to double bounce backscatter. These scatterers hence only are visible for certain sea states and wave conditions. – One more effect should be mentioned. Depending on the sea state the ship will perform pitch and roll movements as well as being lifted or lowered as a whole. In that case the concept of a scatterer having a fixed height above the sea surface will also fail.

All these effects are much too complicated to be treated in this lecture. Here, we will limit ourselves to the simple case of one single reflecting point per scatterer and to scatterers at fixed heights. Some of the analysis will be done using a set of simulated ships in order to show the influence of multipath under controlled conditions. Sets of real measurements will also be used to demonstrate the additional difficulties that occur under real life conditions. Figs.10 and 11 show examples how the RCS of scatterers at different heights, and a complete HRR profile, respectively, vary as a function of range.

The multipath problem has not gained much attention because most ATR approaches are designed for airborne or spaceborne sensors that operate at steeper look-down angles and therefore do not suffer from multipath effects.

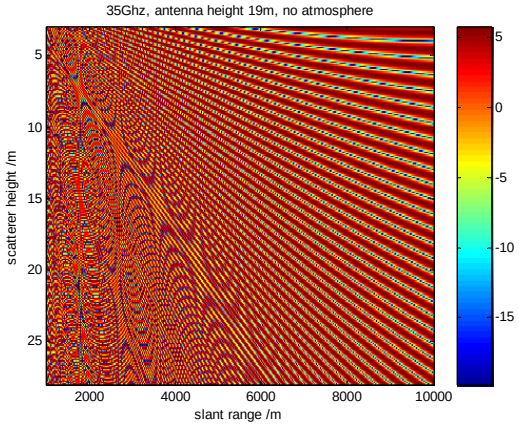

Figure 8: 35GHz propagation factors (dB) for pure multipath, antenna height 19m, scatterer height vs. distance

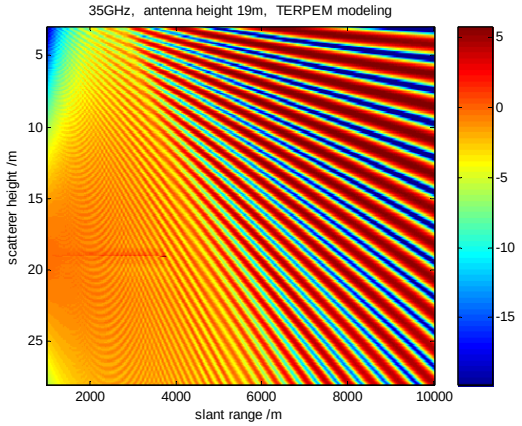

Figure 9: 35GHz propagation factors (dB) including atmospheric effects (TERPEM modeling), antenna height 19m, scatterer height vs. distance

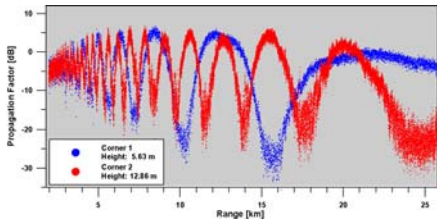

Figure 10: multipath effect on two trihedrals at different heights above the sea surface

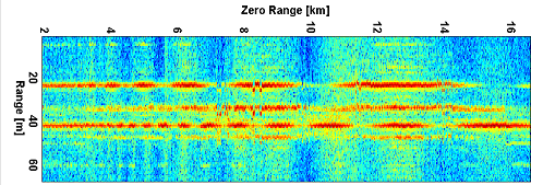

Figure 11: HRR profile of a ship as a function of the slant range between the antenna and the ship, from 2km to 16km, HH polarisation

4.2. The problem of defining testing and training vectors

For classical land targets that have a stable signature it is straightforward to define references that are established by means of some training procedure and subsequently stored in a library. These references may be HRR profiles or ISAR images for pattern matching, or some vector in feature space. Usually these references depend on the aspect angle and have to be defined for all azimuth angles from 0° to 360°, and desirably also for elevation angles out of an interval that is prescribed by the mission parameters. In the case of ships that are subject to multipath this approach will fail because even for a constant aspect angle the signatures will be a function of slant range. One might think to retain the azimuth dependence and replace the elevation dependence (because the depression angles are always close to 0°) by a range dependence thus avoiding to add an additional dimension to the "data dome". The basis for the range dependence could be the geometrical multipath equation as shown in (1) and (2). However, this equation is applicable only for the ideal case of a mirror-like sea surface without any atmospheric influence. In reality, there exists no closed expression by which to include all effects of the sea surface and the conditions of the marine boundary layer. This is only feasible by means of specialised software like TERPEM [5] that requires exact knowledge of important input meteorological parameters like temperature and humidity profiles along the propagation path. These will vary from one mission to another. Moreover, they will not be accessible without the use of meteo buoys. From this one sees that a reference library that includes multipath and atmospheric effects is not feasible and not realistic.

The only way out is to use "true profile" (TP) references that pertain to the undisturbed ship signatures that are not influenced by multipath effects. But then immediately the problem arises that any test vectors that are determined locally will have no resemblance to these TP references and cannot be used together with them to calculate e.g. Euclidian distances in feature space. The task therefore will be to construct test vectors that somehow are an approximation of TP test vectors in order to be comparable to TP reference vectors. In ch.5.3 several approaches will be presented that try to achieve this. It will be found, however, that local approaches (i.e. combining groups of consecutive HRR profiles) are not sufficient to provide stable TP estimates. In ch.6 some possibilities will be discussed how to overcome this systematic shortage by means of rather unusual measures like multi-frequency or multi-antenna systems.

5. RESULTS

5.1. Length estimate

5.1.1. Results for L_a and L_b based on measurements of ship HRR profiles

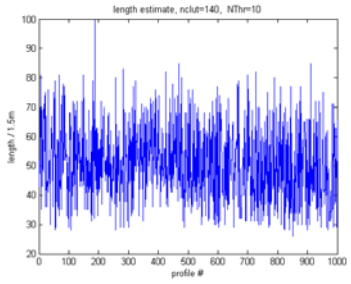

Figure 12: length estimate L_a with distance to ship from 1.2km to 1.4km

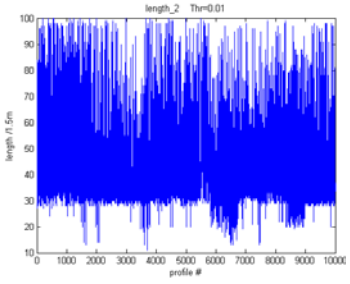

Figure 13: temporal behaviour of L_b

Based on fully polarimetric data that were measured with the MEMPHIS radar at 35GHz [14], several combinations of n_{clut} and N_{Thr} were analysed [3], the one using n_{clut}=140 with N_{Thr}=10 gave the best results. Fig.12 shows the length estimate with its time behaviour and pertinent histogram for the first 1000 HRR profiles (distance to the ship 1.19km to 1.44km). The mean value is 50.7 range cells corresponding to 76 meters, with a standard deviation of 12.6 range cells (18.9 m). This large value reflects the extreme variability of the length estimate (LE). The same behaviour is found for L_b (fig.13). Here again, looking at a large number of profiles yields estimates that show a very strong variability with a mean value of 42.1 cells corresponding to 63.2m (standard deviation =25m) as can be seen from fig.4 for the first 10,000 profiles (distance to the ship from 1.19km to 4.17km).

It is an interesting question what the differences between the results are. From table 1 one can see that for all polarimetric combinations (except the cross-pol case) L_b yields systematically smaller values than L_a. As for X-pol the T/C is smaller than for the "strong" parallel channels, it seems that L_b suffers more from the clutter contribution in the HRR cells. Also, the standard deviations of the LE's are smaller for L_a than for L_b in all cases. From this one can infer that L_a is the more robust approach with values that are closer to the true one than L_b.

The cross correlation coefficient between L_a and L_b is close to zero no matter which polarization channel or combination of channels is used. Of course, the LE values are of the same order of magnitude, but their variations are obviously not correlated which may be due to the the special character of the sea clutter, especially its spikiness.

Table 1: length estimates/meters

	L_a		L_b	
	mean	**std.dev.**	**mean**	**std.dev.**
HH	79.5	16.4	62.9	25.1
VV	76.5	17.0	60.5	23.1
X	64.3	33.1	83.8	36.5
HH+VV	67.7	13.2	57.0	19.1
HH+X	73.2	16.1	59.4	21.2
VV+X	72.4	15.6	58.2	20.2
HH+VV+X	66.4	**12.7**	56.4	**18.4**

The role of polarisation

After applying a careful polarimetric calibration based on so-called "distortion matrices", three independent polarimetric channels are available, namely HH, VV, and the cross-pol channels X=HV=VH. These can be used independently or combined incoherently by summing up the power values. The length estimates (in meters) and especially their standard deviations (cf. table 1) depend strongly on which channel or combination of channels is chosen. As one sees from the standard deviations, the combination of all three

polarisation channels provides the smallest values, i.e. the most stable length estimates (marked by bold type). If only two channels are available then the combination of the two "strong" channels HH+VV is recommended. As to the correctness of the LE, HH+X yields the best results whereas the combination of three channels, although being the most robust one, tends to underestimate the ship's length by about 7 meters.

Table 2		
	Mean(LE)	**std.dev.(LE)**
L_a	65.1m	14.2m
L_b (2%)	40.0m	11.2m
L_b (1%)	46.2m	13.5m
L_b (0.5%)	57.1m	19.7m

Integration of HRR profiles

It has been demonstrated that the two different approaches to estimate a ship's length show a high variability, i.e. rather low robustness. Multipath is only one reason for this, another one being the spiky nature of sea clutter. In addition to polarimetry a second possibility to improve the LE robustness consists in integrating several consecutive HRR profiles by means of incoherently adding their powers. Based on the radar PRF and the ship's outbound velocity an integration of 3 consecutive profiles is possible when the shift is limited to less than about half a range bin [3]. Table 2 gives the results of mean LE and pertinent standard deviations for L_a (parameters n_{clut}=140, N_{Thr}=10 as before) and for L_b with three different thresholds (2%, 1%, and 0.5%).

In the case of L_a the LE is slightly less robust than combining two or three polarimetric channels, but it is clearly more robust than the single channel estimate without integration. L_b on the other hand is obviously too small for threshold values of 1% or 2%. It seems as if the three corner reflectors with their separation of 40 meters that had been mounted on the ship dominate the estimate. For a threshold of 0.5% L_b reaches values around 57 meters as before (but still too small). However, in that case also the standard deviation is around 20 meters as before so that the integration cannot be considered successful.

5.1.2. Simulation of ship HRR profiles

In addition to the measurements, some simulations were made using a "generic" ship that is represented by a dozen main scatterers located at different heights and positions along the length profile of the ship. The cross sections of the scatterers were determined at random between $100m^2$ and $1000m^2$ which are common values for a ship. This layout of scatterers remained fixed for the complete run during which the ship moved away from the radar from a starting distance of 1km to a final distance of 35km with a step size of 10m from one profile to the next based on the TERPEM grid. The effective RCS values of all 12 scatterers varied due to multipath as a function of their height above the water and their distance to the radar (fig.14) as described by the propagation factors that are provided by TERPEM.

Fig.14 (left) shows all profiles between 1km and 35km distance. They were rectified w.r.t. the first profile in order to show the range dependent RCS variation due to multipath for each individual scatterer. The blow-up (Fig.14, center) shows that the stern scatterer is almost invisible between 14.7km and 16km distance, the bow scatterer suffers extinction as well between 16.3km and 17.3km distance. As especially the front and rear scatterers make an important contribution to the estimation of the ship's length, it is expected that the LE will shrink between 14.7km and 17.3km. In the right part of fig.14 is shown as an example how the effective RCS of the stern scatterer behaves as a function of distance. Near the minima the scatterer disappears in the clutter and will not be detectable by any thresholding operation.

The profiles so created were analysed by means of the same algorithms as the measured data. The length estimate L_a (with parameters n_{clut}=400 and N_{Thr}=20 in profiles of length 500 cells) is shown in fig.15 for a sea clutter with σ_0=-25dBm^2/m^2. Due to the benign conditions of the simulation (e.g. no masking effects due to wave height) the results look quite good. As expected the LE is too small in cases where the rear or front scatterers are not discernible like at distances 14km to 18km or beyond 25km.

Fig.15 (center) shows an example of L_b for N_{st}=4 and a threshold of 0.02. The large number of outliers with a tendency to overestimate the LE may be due to sea clutter effects. However, applying a slight median filter of length 7 (right) leads to an efficient decrease of outliers. This shows that one individual estimate may not be very reliable using this approach. An appropriate filter, however, leads to stable values. The median of all 3000 LE values is 39 cells where the correct value would be 40. One also sees very well the expected LE reduction around 15km and beyond 25km, both due to multipath.

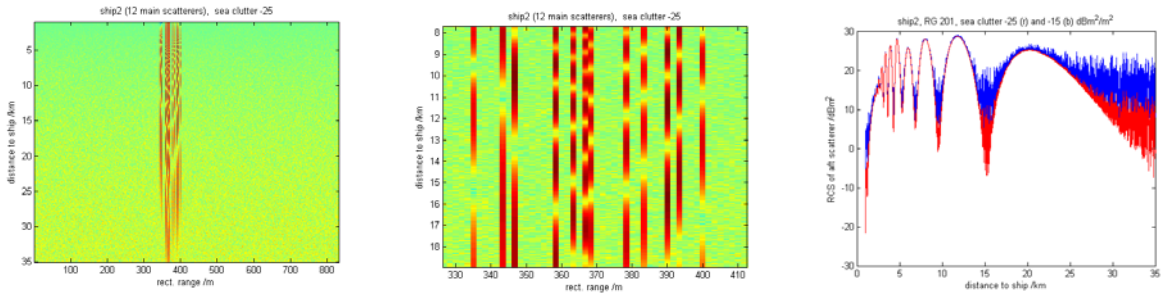

Figure 14: simulated ship HRR profiles modified by multipath

The results demonstrate that the effect of LE fluctuations can be mitigated either by temporal integration or by making use of polarimetry. The latter yields more realistic estimates and provides more samples during each time-on-target. All approaches have in common that the length estimate usually is smaller than the physical/ geometric range extent of the target due to self-masking effects at low depression angles.

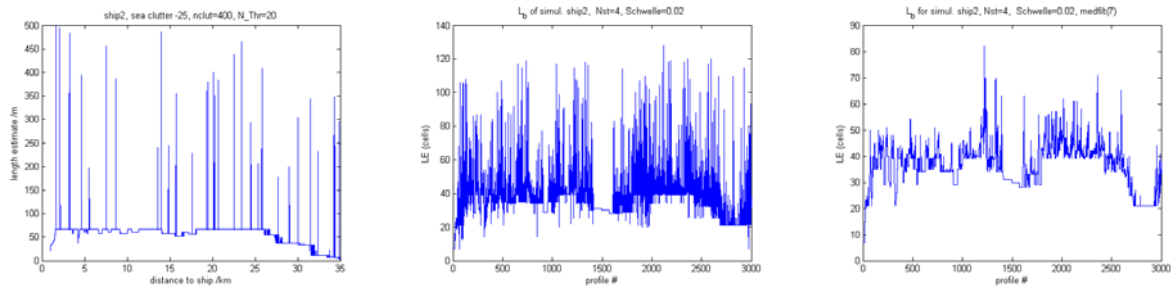

Fig.15 length estimates L_a and L_b based on simulated data with sea clutter σ_0=-25dBm^2/m^2

5.2. PSM results

The PSM scheme described in ch.3.2 was applied to the data of the approaching ship consisting of 400 consecutive HRR profiles of length N_p=208. As we have only data from one single type of ship, i.e. one target class, the PSMs cannot be used for classification at the time being. The goal is rather to study the influence of multipath on the expected classification performance. This is done by testing each of the 400 HRR profiles against some reference PSMs of that same ship. As mentioned earlier, 20 PSMs are constructed at 20 different positions during the ship's approach by subdividing the series of 400 profiles

into 20 packages of 20 profiles each. In addition, an average PSM is created as a mean over all 20 individual PSMs in order to judge how much the variability of HRR profiles due to multipath affects the FoM used for classification.

Fig.16 shows four examples, namely reference PSMs #1, #11, #20, and the averaged PSM. In the upper left, the FoM is plotted for all 400 HRR profiles tested with PSM#1 as reference. The highest FoMs occur at the beginning which is not a surprise as these are the profiles from which reference PSM#1 was constructed. However, only a little further away from these first 20 profiles, the FoM decays continuously to about 2/3 of the original value. This is a clear indication that the variability of the HRR profiles due to multipath is so high that a strong decrease of classification performance has to be expected. Obviously, a reference PSM that is constructed for a certain target is not characteristic for that target at all ranges but only near the position where the reference was established.

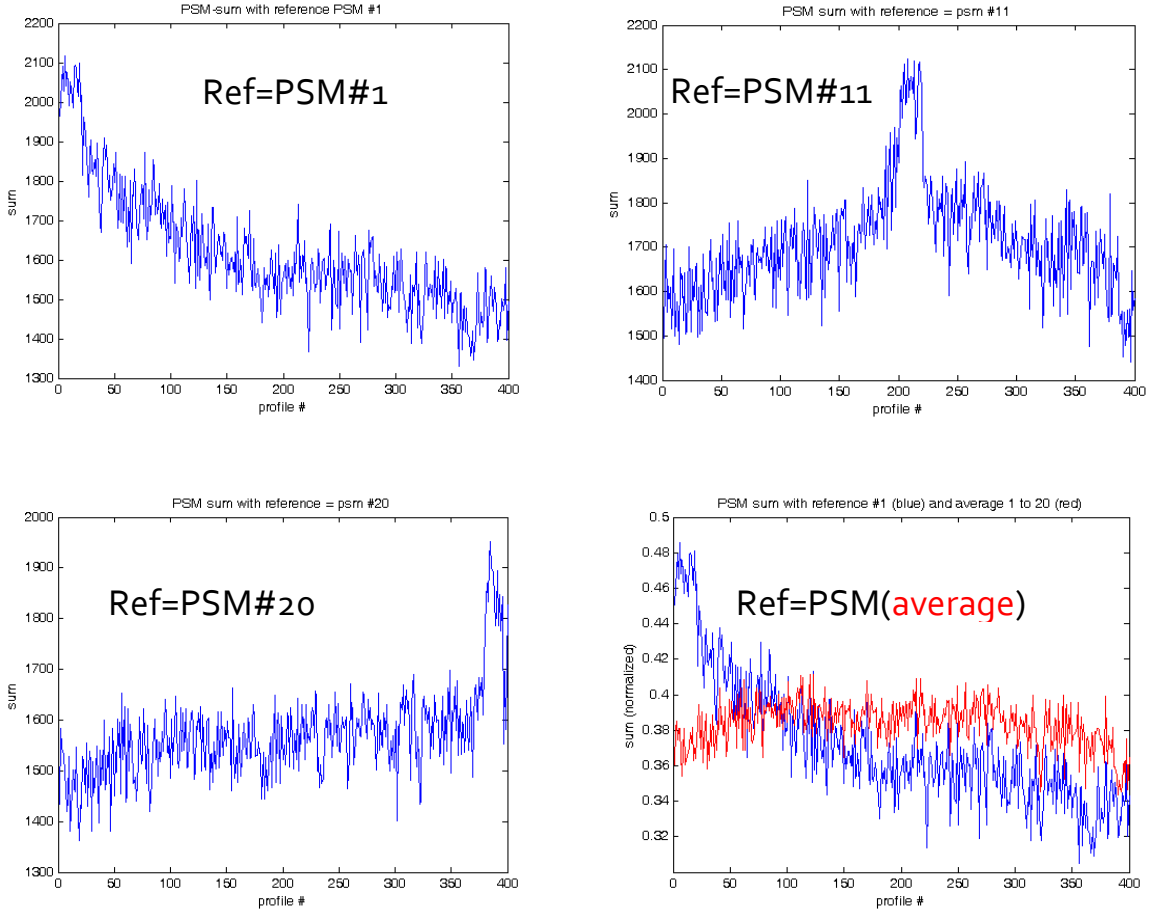

Figure 16: Three examples of the FoM (top and lower left). At the lower right the normalized FoM is shown in a comparison between PSM #1 (blue) and the average PSM (red).

The same result is obtained for the other PSMs #11 and #20 (fig.16, upper right and lower left). The FoM is always highest around the reference range, and decays strongly farther away. If we look at the average PSM (fig.16 lower right, in red) then there is no preferred range any more, i.e. all HRR profiles under test independent of range show more or less the same (dis)similarity to the reference PSM. However, the FoMs reach only 70-80% of the former maximum values and thus likewise demonstrate a loss in classification performance potential.

5.3. Results based on geometrical, statistical, and structural features

5.3.1. Measurements

For this analysis only one ship was available that was measured under controlled conditions at 17GHz. The MARSIG radar [1] was installed fixed on the coast at a height of 19m above the sea surface. In the beginning the trajectory of the target ship was directed away from the radar. After making a turn it approached the radar on a straight course for more than one kilometer at distances between 7.5km and 6.5km. A full circle with a diameter of about 460m concluded the measurement [18]. Here, we analyse the straight course towards the radar under constant front aspect. We select a series of 3600 HRR profiles that cover a total of 900m in distance. In order to analyse how the HRR signature of the ship varies, six groups of 100 profiles each are extracted with a distance separation of about 160m between each group. The 6 groups are B2, B8, B13, B16, B21, and B27, extracted from a total of 27 groups. Fig.17 shows three examples that are taken from near the beginning, near the center part, and near the end of the straight trajectory. It is striking that there is hardly any similarity between the three groups. Although the front aspect of the ship was constant during the approach it seems as if its length did change. Obviously some of the scatterers near the bow and the stern that had disappeared due to multipath at far distance reappeared during the approach thus giving the impression of increased range extent. Also, looking at B13 as an example of one individual group (fig.17 center) one can distinguish strong variability of individual scatterers although each group represents a distance interval of only 25m. The scatterer near the bow shows four well defined maxima, the scatterer near range gate #380 shows a strong maximum between profiles 1480 and 1500, and a pronounced oscillation in earlier profiles. Obviously it cannot be expected that a training feature set that was calculated at a certain distance will work well at a different distance.

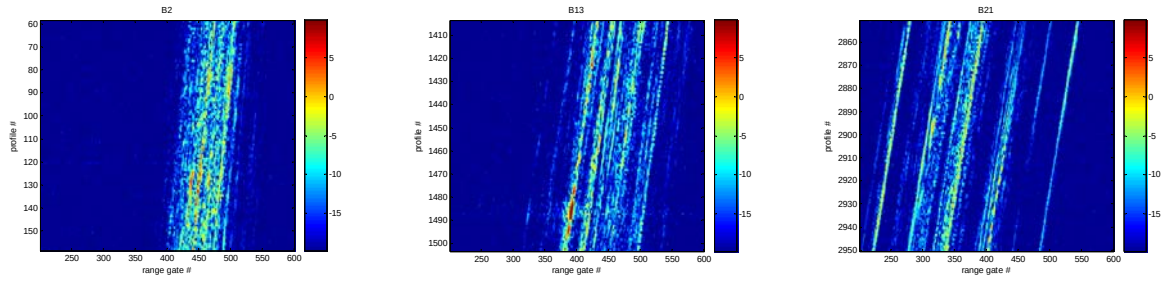

Figure 17: measured HRR profiles (dB) for three distance intervals B2, B13, B21 (100 profiles corresponding to 25m) lying about 350m apart

In the following we will look how ATR test features vary within each group and from one group to the other. Next, reference features will be determined as the outcome of a training procedure. Two different approaches will be compared to each other. Finally, the feature references and the local test features will be used to classify the six groups against each other. Each group will be treated as a different target for this analysis. If the confusion matrices are “flat” this would mean that the groups cannot be distinguished from each other, i.e. that the influence of multipath (and propagation effects) is not strong enough to change the ship’s HRR signature significantly. On the other hand, if the confusion matrices show a pronounced “ridge” in the main diagonal, this means that multipath will have a strong influence on ATR performance.

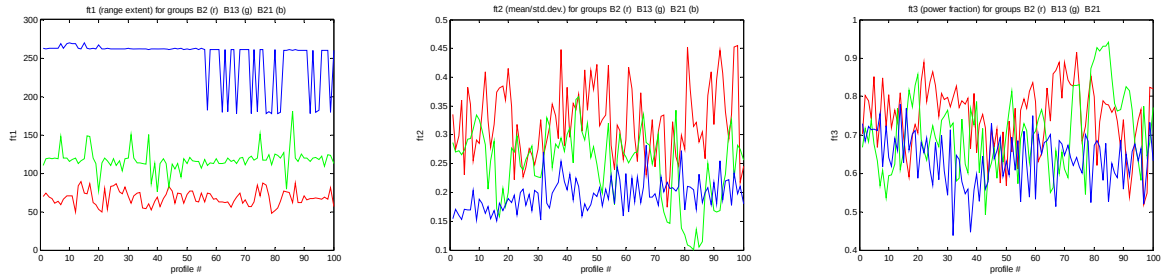

Figure 18: comparison of feature history of features ft1 (left, ft2 (center) and ft3 (right) for three distance intervals B2 (r), B13 (g), B21 (b)

For the same three groups as in fig.17, fig.18 shows the behaviour of features ft1, ft2 and ft3 across the 100 profiles of each group. In order to calculate the feature values, the original HRR profiles were processed to generate well defined peaks as described in chapter 2. The most stable and most distinctive one is the geometrical feature ft1 (range extent) which essentially describes what can be seen in fig.17. All other features show much stronger fluctuations with larger overlaps of their histograms, ft2 and ft3 being typical examples (fig.18). The strong fluctuations of the local feature values reflect the similarly strong variations of the HRR profiles from which they are derived.

For classification purposes one needs feature references that are the result of some training procedure. As we do not have any independent measurements we have to determine these references from each group of HRR profiles individually. The feature values that are derived from individual HRR profiles are considered test values, i.e. there are 100 test values per group as shown in fig.15. The training values have to be somehow representative of all of them, therefore they should be based on one “reference profile” that represents its group. There are two possibilities to determine such a reference profile as described in chapter 2. One is to average all RCS values within each range cell, the second one is to retain the maximum value within each range cell (“maxing”). Of course, all 100 profiles have to be carefully aligned for both approaches. The averaging process will lead to lower RCS values as compared to the “true” profile (i.e. undisturbed by multipath effects), the “maxing” process may lead to higher RCS values (up to 6dB depending on the reflectance of the sea surface). This does not matter because the calculation of the features only depends on relative RCS values. The question therefore is how the two approaches influence the RCS relations between the scatterers. There is no simple answer to this because it depends on the distance to the ship and on the height of each scatterer as can be seen from the propagation factor diagrams (figs.8 and 9). The faster the fluctuation the more likely the “maxing” will lead to a stable reference profile. For a rough surface with a higher sea state leading to stronger motion of the ship, the single reflection multipath mechanism will no longer be realistic (cf. chapter 4.1). In that case the averaging approach may lead to a better reference profile.

These training references are now used together with the 100 test values from each group to construct confusion matrices by trying to classify the six groups against each other. Four sets of features are analysed here: Set #1 (features 1 4 8 14), set #2 (features 2 6 14), set #3 (features 7 11 14), set #4 (features 1 2 3 4 5 6 7). Sets 1 through 3 are composed of mainly uncorrelated features while set #4 disregards any possible correlation. Fig.19 shows a comparison between the (colour-coded) confusion matrices of all 4 sets using the AV references (upper row) and the MX references.

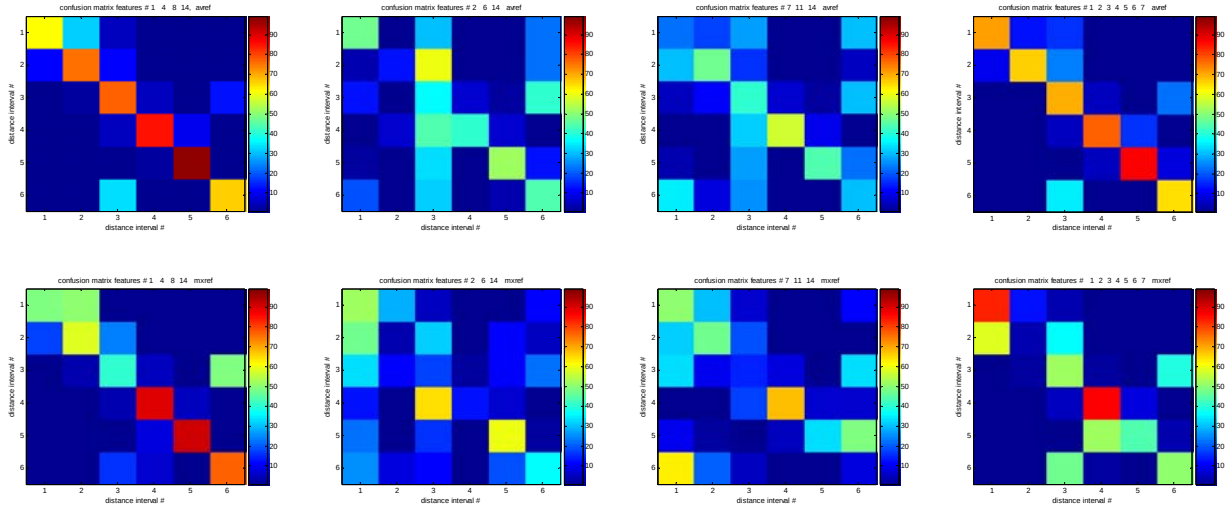

Figure 19: confusion matrices (%) between 6 distance intervals for 4 sets of features with feature references obtained by averaging (top row) and by maxing (bottom row)

Table 3 summarizes the P_{cc} percentages from the main diagonal of all eight confusion matrices:

Table 3 P_{cc}(%) values from main diagonal of confusion matrices

distance interval	*averaging reference*				*maxing reference*			
	Set 1	***Set 2***	***Set 3***	***Set 4***	***Set 1***	***Set 2***	***Set 3***	***Set 4***
1 (B2)	62	47	23	71	49	53	51	83
2 (B8)	76	13	47	66	58	4	48	4
3 (B13)	77	36	42	70	41	18	15	53
4 (B16)	85	42	57	77	90	14	68	87
5 (B21)	97	52	44	87	92	60	33	44
6 (B27)	66	45	31	65	77	36	9	51
average	77.2	39.2	40.7	72.7	67.8	30.8	37.3	53.7

One sees that the different feature sets show quite different classification performance. One should emphasize, however, that the task is not to find a set of best features for ship classification. Rather, the task is to demonstrate that there exist (sets of) features that are able to distinguish between the HRR signatures of the same ship at different distances. This means that the classification of this ship (and consequently any ship) against other ships will most likely fail. Both “successful” feature sets (1 and 4) contain the “range extent” (ft1). This may be a hint that it is mainly the geometry that suffers from multipath while statistical and structural features show less distinction. Comparing both rows of fig.19, i.e. AV and MX references, one may conclude that averaging seems to be more advantageous than “maxing” in the case of real ship measurements, i.e. for real life applications.

5.3.2. Classification based on simulated ships

A group of five ships (S1,…,S5) was simulated as described in [21]. It contains 3 long and 2 shorter ships, one rather high ship, two medium high ships, and two with height up to 10m. S1 is identical to the simulated ship used in ch.5.1.2. In order to determine the classification performance, the 5 ships moved

away from the radar starting at 1km distance, and ending at 9km distance. Every 10m a HRR profile was determined on the basis of the scatterers' geometry and the propagation factors that were calculated using TERPEM with an antenna height of 19m above the sea surface. Consequently, for each ship 800 HRR profiles were available from which 800 values for each of the 14 features were determined. Figs.20 and 21 show examples for ship S3 which is 60m long but rather flat with no scatterer higher than 10m.

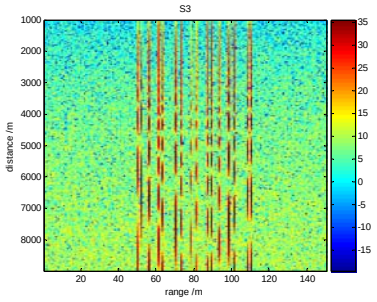

Figure 20: aligned HRR profiles (dB) of ship S3 for distances from 1km to 9km

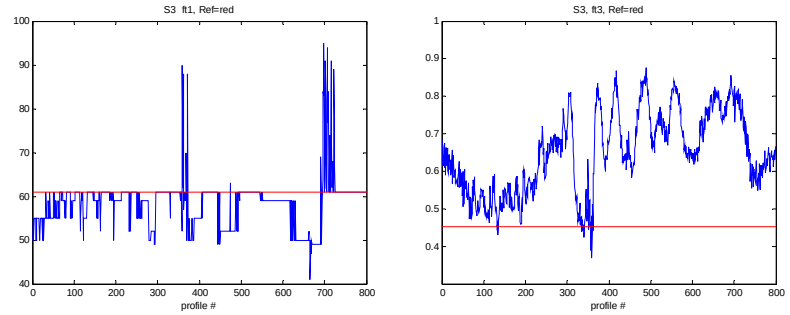

Figure 21: values of features 1 & 3 (ship S3) as a function of distance (red line = reference from table 2)

As can be seen from figs.21 the local feature values differ considerably from the "true profile" references (red line). This is true for all 14 features, the range extent (ft1) being one of the moderate examples. Consequently, it cannot be hoped that the single profile feature values will perform well when used for classification. Based on the cross correlation between features (fig.4), three sets of features were selected for classification, set #1 consisting of features 1, 4, 8, and 14, set #2 consisting of features 2, 6, and 14, and set #3 consisting of features 7, 11, and 14. For all three sets, confusion matrices between all 5 ships were constructed based on all 800 HRR profiles. The results did in no case show a pronounced main diagonal as expected. The question is how one can extract better test feature vectors from the available data. One possibility is the formerly mentioned method of grouping several consecutive HRR profiles either by averaging or by "maxing".

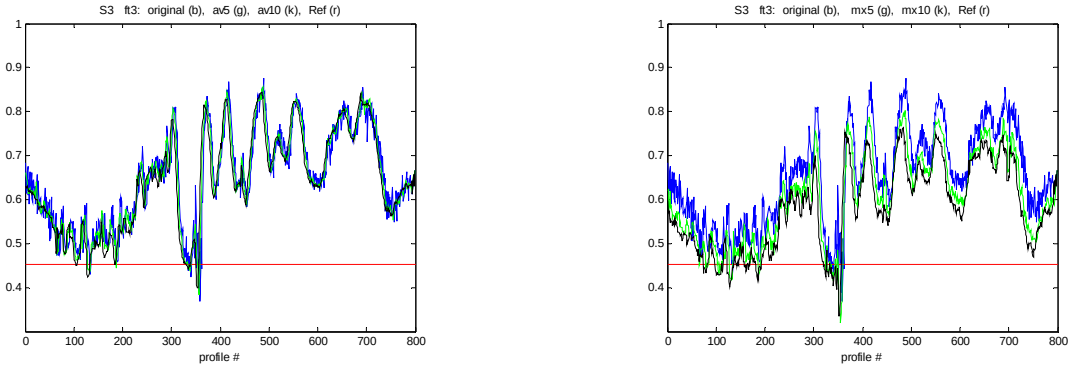

Figure 22: comparison of different ways to compute the test features (S3, ft3): averaging (left) or maxing (right) for L=1 (blue), L=5 (green), L=10 (black) (red line = overall reference)

When we look at how the local feature estimates (i.e. test features) change depending on averaging or maxing we find as expected a tendency to come closer to the overall reference. Fig.22 shows feature #3 of S1 as an example. The effect is more pronounced for maxing (right) than for averaging (left), and it increases with the number L of profiles that are grouped together. The examples show L=5 (green) and L=10 (black).

One may now go back to calculating confusion matrices based on the modified feature estimates that one gets from averaging or "maxing" groups of L consecutive profiles. As it is not possible to show all the matrices here, and as we are mainly interested in the main diagonal, these values are shown in table 4 for the feature set ft1, ft4, ft8, ft14.

Table 4 main diagonal values (%) of confusion matrices for five different approaches to calculate the test features (feature set fts 1, 4, 8, 14), "true profile" reference

	orig	***av5***	***av10***	***mx5***	***mx10***
S1	68.6	67.5	67.5	67.0	64.0
S2	9.0	8.1	9.1	12.0	13.1
S3	15.1	15.4	18.3	18.0	23.3
S4	27.3	27.1	29.1	32.1	38.5
S5	64.5	71.1	72.6	66.6	67.6
average	36.9	37.8	39.3	39.1	**41.3**

Listed are the percentages of correct classification of each of the five simulated ships. The first column gives the P_{cc} values based on test features that are derived from individual HRR profiles. Columns 2 and 3 show P_{cc} values based on test features that are derived from 5fold and 10fold averaged HRR profiles, respectively. Finally, columns 4 and 5 show P_{cc} values based on test features that are derived from 5fold and 10fold "maxed" profiles. In all cases, the "true profile" reference feature vector was used. As one sees, the "good" classification of S1 has a tendency to become slightly worse while all the others show an improvement which is more pronounced for "maxing" than for averaging. Also, larger L is better than smaller L. Still, the classification results are not satisfactory.

We already discussed that in the case of real ships the "true profile" (TP) is not necessarily known (only when the ship is known from a signature library), and that it may be required to obtain an estimate from all available observations. It may even be advantageous to use such an estimate instead of the "true profile" reference because the true profile actually is never seen during a real measurement. This explains the large deviation between local feature estimates and the TP reference as shown in figs.21 and 22. We therefore determine two alternative feature references that are based on averaging and "maxing" all 800 HRR profiles, i.e. using an 8km observation distance interval. This is a rather favourite assumption, as in a real life scenario the available distance intervals will tend to be shorter mainly due to time constraints before making a decision. Table 5 shows the respective P_{cc} values (%), again only for the main diagonal of the confusion matrices using the same feature set as before.

Table 5 main diagonal values (%) of confusion matrices for three different ways to determine the test features (HRR profiles original / averaged L=10 / "maxed" L=10) combined with two ways (averaging / maxing all 800 HRR profiles) to determine the feature reference

Ship	***original***		***averaging L=10***		***maxing L=10***	
	avref	***mxref***	***avref***	***mxref***	***avref***	***mxref***
S1	77.3	62.8	75.5	56.4	71.3	53.4
S2	8.5	21.9	8.5	22.4	13.4	25.0
S3	9.8	22.8	11.3	22.1	14.9	30.1
S4	18.6	18.5	17.4	20.6	28.1	28.9
S5	73.5	78.5	83.1	88.6	79.9	84.3
average	37.5	40.9	39.2	42.0	41.5	**44.3**

The terms in row one refer to the way the test feature values are computed, i.e. from original individual HRR profiles or from 10fold averaged or 10fold "maxed" HRR profiles. Each of these three cases is combined with the two possibilities of choosing the overall reference, either by averaging ("avref") or by "maxing ("mxref"). There is no clear tendency to be inferred from tables 4 and 5. For ships S1 and S4, using the TP reference seems best whereas for S2, S3 and S5 using the "mxref" yields the best results. Therefore it might be best to look at the average P_{cc} values in the last line which summarize the results for all 5 ships. The highest value (44.3%) is reached for test feature vectors derived from maxing with L=10, together with a feature reference that also was obtained by means of maxing. This is in contradiction to the findings from ch.5.3.1 based on measurements. To which extent this depends on the properties of the sea surface remains an open question. It may well be that the smoother the sea surface is, the more realistic the "maxing" reference profile may become.

6. THE MITIGATION OF MULTIPATH EFFECTS ON SHIP ATR

The results from ch.5 show that TP references and local test vectors do not fit together. Trying to approximate true profiles by local operations like averaging or maxing shows a certain improvement but is not sufficient. On the other hand (ch.5.3.1, 5.3.2) using references that are obtained from a limited observation interval instead of TP references showed considerable improvement in classification performance. However, these references cannot be established ahead and stored in a reference library. This leads to the conclusion that there is no way around TP references for ship classification. The main difficulty is then to obtain a realistic test feature vector that can be compared to the stored "true" reference feature vector for the classification process. This can only be achieved by filling the "gaps" in the propagation factor diagram in order to eliminate excessive oscillations of the scatterer amplitudes.

The multipath formula (2) takes into account the surface roughness via a reduced reflectivity by introducing a factor $f \in [\ 0\ \ 1]$. For complete reflection (f=1) the resulting voltage may assume values between 0 (extinction) and 2 which corresponds to a 6dB increase in received power. For f<1 the extinction is less pronounced, and the gaps that have to be filled are less deep. A typical example of the propagation factor (V^2|dB) is shown in fig.23. From this one sees that the oscillation between minima and maxima is the faster (i.e. the gaps are narrower) the closer the ship is to the antenna.

Looking at the propagation factor diagrams offers several possibilities to arrive at stable HRR profile estimates, i.e. to obtain a successful filling of the gaps of extinction. Clearly this requires properly integrating several profiles that have their minima and maxima at disjoint positions. From (2) one sees that this can be done by varying either Δ or λ. The latter would mean to use a multi-frequency radar that is able to switch its frequency from pulse to pulse or from sweep to sweep (for a rotating antenna). Varying Δ offers two more possibilities, namely to vary either the antenna height H or the slant range "s" for a fixed scatterer height h.

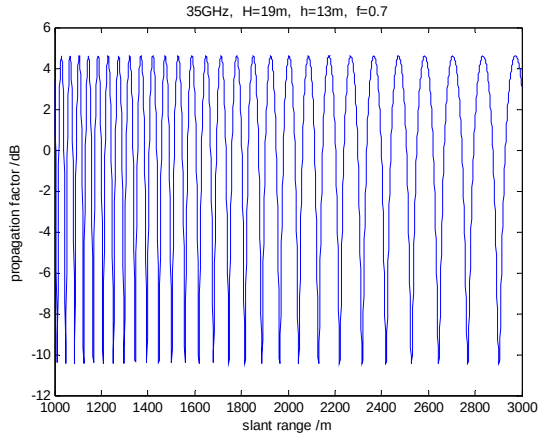

Figure 23: geometric multipath propagation factor at 35GHz for H=19m, h=13m, f=0.7

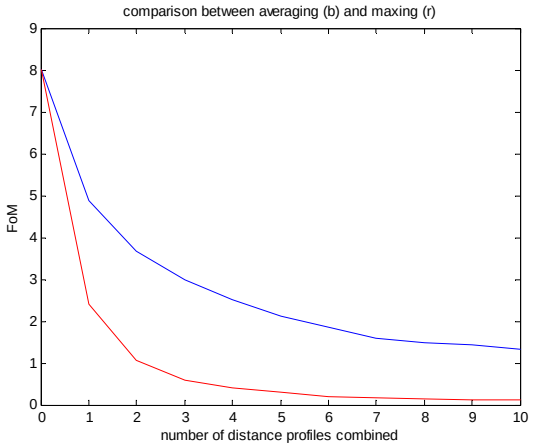

Figure 24: FoM obtained by combining n=1…10 profiles with the original profile by means of averaging (blue) or "maxing" (red)

Varying "s" is equivalent to temporal integration as long as the ship that has to be classified is approaching the antenna or receding from it. Of course, the antenna height H can normally not be changed. But it is imaginable to use two or three antennas at different heights and to alternately transmit and receive with them. It can be shown that height differences of less than 1m are sufficient to achieve a considerable improvement in the HRR profile estimates. Fig.24 gives an example where the standard deviation of the result of combining up to ten distance profiles (i.e. as seen from up to ten antennas at different heights) was used as a figure of merit (FoM) in order to quantify the smoothing success. As one sees, a significant reduction is already obtained by combining only three profiles which seems feasible in practice. Different ways to combine the profiles were analysed. Averaging (in dB space) was less successful (blue curve) than "maxing" (red) i.e. retaining the maximum of any two values to be combined. It is obvious that this approach will also provide HRR profiles that are more similar to the "true" (i.e. without multipath) profile of the ship and hence will result in more realistic estimates of the test feature vector and better classification results.

7. SUMMARY

Based on real measurements (at 17GHz and 35GHz) and simulations (at 35GHz) of ship HRR profiles it was shown how the influence of multipath and propagation effects at shallow depression angles will inevitably lead to a strong variability of the ship's signature as a function of distance. This variability will affect HRR profiles as well as ISAR images both of which are the basis to construct ATR features. Two different approaches (averaging and "maxing") to establish stable test HRR profiles were analysed. None of them is optimum and comparable to TP reference profiles. Also, estimates of reference profiles from longer observation intervals as an approximation to "true profiles" were analysed. They show an increase in classification performance, however, they are not suitable to be stored in a reference library as a surrogate for the true profiles. When the latter are used as references, the main problem remains with the test features that are derived from single HRR profiles and naturally show the same strong fluctuation as these. A temporal integration of several consecutive HRR profiles leads to a certain stabilization of the test features and results in improved ATR performance [3]. However, this is not sufficient, and moreover time may be a critical issue. New approaches [20] are mainly aimed at filling the "gaps" of the propagation factor diagram either by operating at several radar frequencies or with several antennas at different heights. Technically, both approaches can easily be realized. Two frequencies and/or three antenna heights seem sufficient to achieve a substantial improvement in ATR performance without causing excessive additional cost.

8. REFERENCES

[1] H.Essen, H.- H. Fuchs, R.Sommer, A.Wahlen, W.Johannes, D.Janssen, MARSIG, Entwicklung eines Experimentalradars für Schiffs-Signaturmessungen, FGAN-FHR Jahresbericht 2008, p.102-104

[2] H. Essen, H.-H. Fuchs, G. Lindquist, A. Pagels, Influence of Atmospheric Propagation in the Maritime Boundary Layer on the Measured RCS of Ships, Proc. SPIE Conf. Remote Sensing, Vol. 7476-02, Berlin, Germany, 31 Aug.- 3 Sept. 2009

[3] Schimpf, H., Fuchs, H.-H., The Influence of Multipath on the Classification of Ships, Proc. Int'l Radar Symposium IRS 2009, Hamburg, Germany, 9-11 Sept. 2009, p.597

[4] Schimpf, H., Dessauvagie T., The estimation of target length from radar high range resolution profiles, FGAN-FHR Technical Report #54 (05-2003), Wachtberg, Mai 2003

[5] TERPEM User Guide, 2nd edition, Signal Science Ltd., Abingdon, UK, Dec. 2005

[6] Pastina, D., Lombardo, P., Farina, A., Daddi, P., Super-resolution of polarimetric SAR images of ship targets, Signal Processing 83 (2003), 1737 – 1748

[7] Sciotti, M., Pastina, D., Lombardo, P., Exploiting the polarimetric information for the detection of ship targets in non-homogeneous SAR images

[8] Panagopoulos, G., Tsagaris, V., Anastassopoulos, V., Using synthetic aperture radar data to detect and identify ships, SPIE online Doc.#10.1117/2.1200802.1062 (2008)

[9] Margarit, G., Mallorqí, J.J., Fábregas, X., Single-Pass Polarimetric SAR Interferometry for Vessel Classification, IEEE-GRS 45,11 (Nov.2007), 3494 – 3502

[10] Bon, N., Hajduch, G., Khenchaf, a., garello, R., Quellec, J.-M., Recent developments in detection, imaging and classification for airborne maritime surveillance, IET Signal Processing, 2008, Vol.2 No.3, pp.192 – 203

[11] Menon, M.M., Boudreau, E.R., Kolodzy, P.J., An Automatic Ship Classification System for ISAR Imagery, The Lincoln Laboratory Journal 6(1993), pp.289 – 308

[12] Touzi, R., Raney, R.K., Charbonneau, F., On the Use of Permanent Symmetric Scatterers for Ship Characterization, IEEE-GRS 42,10 (Oct.2004), pp.2039 – 2045

[13] Cotuk, N., Ture, S., Cetin, M., Application of point enhancement technique for ship target recognition by HRR, SPIE Proceedings Vol. 5095 "Algorithms for Synthetic Aperture Radar Imagery", pp.185-193, September 2003

[14] H.Schimpf, H.Essen, S.Boehmsdorff, T.Brehm, MEMPHIS – a Fully Polarimetric Experimental Radar, Proc.IGARSS 2002, Toronto, Canada, June 2002

[15] Pastina D., Spina C., Multi-feature based automatic recognition of ship targets in ISAR, IET Radar Sonar Navigation, 2009 Vol.3, pp.406- 423

[16] Pastina D., Spina C., Multi-feature based automatic recognition of ship targets in ISAR images, Proc.2008 IEEE Radar Conf., Rome, Italy, May 2008

[17] Musman S., Kerr D., Bachmann C., Automatic recognition of ISAR ship images, IEEETrans. AES 1996, Vol.32, pp. 1392 – 1404

[18] Schimpf H., Fuchs H.-H., Analysis of ATR Features for non-cooperative ground-based Classification of Ships, Proc. Int'l Radar Symposium IRS 2010, Vilnius, Lithuania, 16-18 June 2010, pp. 148 – 152

[19] Schimpf H., Fuchs H.-H., Maresch A.,The Classification of Ships in the Presence of Multipath, NATO-Symposium SET-160 on "NCI/ATR in Air Ground and Maritime Applications Based on Radar and Acoustics", Athens, Greece, 11-12 October 2010, #20

[20] Schimpf H., The Mitigation of the Influence of Multipath on the ground-based Classification of Ships, Proc. Int'l Radar Symposium IRS 2011, Leipzig, Germany, 7 – 9 Sept 2011, to be published

[21] Schimpf H., The Influence of Multipath on Ship ATR Performance, SPIE Proceedings Vol. 8049, paper #38, "Defense, Security, and Sensing 2011" Conference, Orlando, FL, April 2011